Full title: Strain and Vector-Magnetic-Field Tuning of the Anomalous Phase in $Sr_3Ru_2O_7$.

Short title: Symmetry of the Anomalous Phase in $Sr_3Ru_2O_7$.

Daniel O. Brodsky[1,2], Mark E. Barber[1,2], Jan A. N. Bruin[2,3], Rodolfo A. Borzi[4], Santiago A. Grigera[2,4], Robin S. Perry[5], Andrew P. Mackenzie[1,2], Clifford W. Hicks[1,*]

[1]Max Planck Institute for Chemical Physics of Solids, Nöthnitzer Straße 40, 01187 Dresden, Germany

[2]Scottish Universities Physics Alliance (SUPA), School of Physics and Astronomy, North Haugh, University of St. Andrews, St. Andrews KY16 9SS, United Kingdom

[3]Max Planck Institute for Solid State Physics, Heisenbergstraße 1, 70569 Stuttgart, Germany

[4]Instituto de Física de Líquidos y Sistemas Biológicos (IFLySIB), UNLP-CONICET, 1900 La Plata, Argentina

[5]London Centre for Nanotechnology, University College London, Gower Street, London WC1E 6BT, United Kingdom

[*]Corresponding author

February 2016

arXiv:1512.04216v2 [cond-mat.str-el] 22 Feb 2016

Symmetry is a basic paradigm for analysis of problems in solid state physics, and to controllably break point-group symmetries is a powerful probe of novel forms of order. In this work, we apply two methods, controlled lattice strain and vector magnetic field, to study a well-known correlated electron phase that appears at low temperatures in the layered material $Sr_3Ru_2O_7$. This phase responds strongly to C_4-symmetry-breaking fields, suggesting spontaneous C_4 symmetry breaking. However in this work we find that the data are explainable with microscopic coexistence of two perpendicular order parameter components, which, though not strictly ruling out spontaneous C_2 symmetry, implies local C_4 (or possibly D_{2d}) symmetry in the absence of C_4-symmetry-breaking fields. The techniques presented in this work will be relevant for other systems where spontaneous C_4 symmetry breaking is suspected.

Introduction

$Sr_3Ru_2O_7$ is a layered perovskite metal in which conduction takes place in Ru-O bilayers. Interlayer coupling leads to substantial bilayer splitting of parts of the electronic structure, but the bilayers are weakly coupled, and the Fermi surfaces are quasi-two-dimensional. [1, 2] Electronic correlations are strong, as evidenced by a large mass renormalization and Wilson ratio, [2, 3] inelastic neutron scattering data, [4] and the induction of localized spin density wave order by certain impurities. [5, 6]

The strongest focus of interest in $Sr_3Ru_2O_7$ has been on an anomalous phase that condenses below 1.1 K, in a narrow window of magnetic field **H** around 8 T when **H** is close to the crystallographic c axis. [7] A defining feature of this phase is strong enhancement of the in-plane resistivity. The physics in this region of field and temperature is highly purity-dependent; the anomalous phase does not appear if the residual resistivity exceeds $\sim$1 $\mu\Omega$-cm. [8] In samples not far above this limit, a single metamagnetic transition is seen at 8 T whose critical endpoint is located at $\sim$0 K. [9] In cleaner samples, that show phase for-

mation, this metamagnetic transition bifurcates into two first-order transitions, at ≈7.9 and ≈8.1 T and with respective critical endpoints at 0.7 and 0.6 K. Condensation of the phase therefore appears to be intertwined with the metamagnetism, and the critical endpoints of the metamagnetism; [10, 11, 12, 13, 14] the phase appears to mask what would otherwise be a bare $T \sim 0$ critical endpoint, that is, a quantum critical endpoint.

This relationship between phase formation and quantum criticality, in a system that can be grown with exceptionally low disorder, has been a major motivation of interest in $Sr_3Ru_2O_7$. Another major source of interest has been the possibility that, through the effects of electronic interactions alone, phase formation reduces the point group symmetry of the system from C_4 (tetragonal) to C_2 (orthorhombic). [7, 15] (Throughout this work, we use the tetragonal unit cell of $Sr_3Ru_2O_7$. [16]) Whether this symmetry reduction truly occurs or not is a question of broad importance because of the growing range of materials in which electronic interactions are suspected or demonstrated to drive a C_4 to C_2 transition. Examples include underdoped $YBa_2Cu_3O_{6+x}$, [17, 18], iron pnictide superconductors, [19, 20] a nematic quantum Hall state in GaAs 2D electron gases, [21, 22] and the hidden order phase of URu_2Si_2. [23] In $Sr_3Ru_2O_7$, the principle motivation to consider a C_4 to C_2 symmetry is a pair of observations. (1) The resistivity enhancement in the phase, at ∼100%, is surprisingly strong, suggesting an additional scattering channel which could be domain walls. [8] (2) When $\mathbf{H}$ is tilted modestly towards a $\langle 100 \rangle$ direction, the resistivity within the phase becomes strongly anisotropic, suggesting that the in-plane component of the field is orienting domains, or domain walls. [15] To explain these observations, several models for nematic Fermi surface distortions in $Sr_3Ru_2O_7$ have been proposed. [24, 25, 26, 27, 28]

A recent landmark neutron scattering study found density wave order within the phase: there are scattering peaks at $(\pm q, 0, 0)$ and $(0, \pm q, 0)$, with q incommensurate and taking on slightly different values above and below the second metamagnetic transition (at 8.1 T). [29] The observed phase boundaries are in excellent agreement with those seen in transport and thermodynamic studies. [8] Most of the models for nematicity in $Sr_3Ru_2O_7$ are based on $q = 0$ inter- and intra-orbital interactions, and while it remains possible that such interactions play an important role in phase formation, the neutron data establish that $q \neq 0$ interactions are also present and translation symmetry is broken within the phase.

The scattering peaks are C_4 symmetric (when $\mathbf{H} \parallel \hat{\mathbf{c}}$): the peaks at $(\pm q, 0, 0)$ and $(0, \pm q, 0)$ have equal magnitude. Similarly, all measurements of resistivity to date have shown in-plane isotropy when $\mathbf{H} \parallel \hat{\mathbf{c}}$. This macroscopic C_4 symmetry could result either from microscopic C_4 symmetry, or averaging over domains of locally C_2-symmetric order. (A third possible point group symmetry, D_{2d}, is considered in the Discussion.) With respect to the density wave order, the question of C_4 versus C_2 symmetry is that of whether the perpendicular components coexist microscopically, forming a checkerboard-type order, or in separate domains. Extensive thermodynamic studies of $Sr_3Ru_2O_7$ have shown that the transition into the phase with temperature, at 1.1 K for $\mu_0 H \approx 7.9$ T, is second-order, [8, 30, 31] so it is expected that the phase lifts at least one symmetry of the underlying lattice. It could be translation symmetry alone, or translation and C_4 together.

This question is studied here through measurements of the in-plane resistivities ρ_{aa} and ρ_{bb} against applied C_2-symmetric fields: anisotropic strain and vector magnetic field. With spontaneous C_2 symmetry, in principle an arbitrarily small C_2-symmetric field orients the ground state. Therefore a discontinuity in the ground-state ρ_{aa} and ρ_{bb} is expected, as the C_2

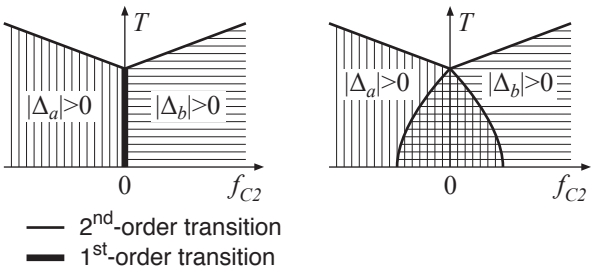

Figure 1: Two generic possible phase diagrams of a two-component order parameter, where each component is C_2 symmetric. T is temperature and f_{C2} a C_2-symmetric field. $f_{C2} < 0$ favors (100)-oriented component Δ_a, and $f_{C2} > 0$ favors (010)-oriented component Δ_b. In the left-hand diagram, Δ_a and Δ_b compete strongly and do not coexist; at $f_{C2} \sim 0$ domains of locally C_2-symmetric order may form. In the right-hand diagram, Δ_a and Δ_b can coexist, and at $f_{C2} = 0$ the system is C_4 symmetric.

field is tuned through zero and the favored orientation flips. In contrast, without spontaneous C_4 symmetry breaking all ground-state properties should vary continuously with applied C_2 field.

However a C_4-symmetric state could still have a high susceptibility to C_2 fields, such that $\rho_{aa} - \rho_{bb}$ grows rapidly but continuously with applied C_2 field: it is important to distinguish this possibility from an actual discontinuity. Testing a range of applied C_2 fields is highly useful, to isolate extrinsic effects. For example, an inadvertent internal field, such as anisotropic strain applied by the sample mount or oriented dislocations, could shift the possible discontinuity away from zero applied C_2 field. It could also be rounded out by domain formation; which has been the prevailing hypothesis for $Sr_3Ru_2O_7$. [15, 32, 29] Domains in the ground state could occur due to to random-field disorder, or long-range interactions. If, for example, an electronic C_2 state induces a strong C_2 lattice distortion, but the sample is rigidly mounted, long-range elastic interactions will favor domain formation.

The neutron study (Ref. [29]) suggests that the phase can be described in two-component framework, where the amplitude of the (100)-oriented density wave is $|\Delta_a|$, and the (010)-oriented density wave $|\Delta_b|$. Tilting $\mathbf{H}$ towards $\hat{\mathbf{a}}$ suppresses both the (010) density wave amplitude and the enhancement in ρ_{bb}, suggesting that the enhancement of ρ_{bb} is a monotonic function of $|\Delta_b|^2$, and likewise ρ_{aa} enhancement is a monotonic function of $|\Delta_a|^2$. Within a two-component framework, a lowest-order free energy analysis provides a clear distinction between C_4-symmetric and spontaneously C_2-symmetric order: spontaneous C_2 symmetry results when the interaction energy between Δ_a and Δ_b is high enough that they cannot both be nonzero in the ground state. [33] In this case the transition between nonzero Δ_a and nonzero Δ_b is first-order, allowing domain formation and metastability. On the other hand, with sufficiently low interaction energy, there is a nonzero range of applied C_2 field, bounded by second-order transitions, over which both components have nonzero amplitude. These two possibilities are illustrated with the phase diagrams shown in Fig. 1, and the aim of this work is to determine which diagram, if either, is more applicable to $Sr_3Ru_2O_7$.

Results: strain-tuning

It has previously been found that hydrostatic pressure increases the metamagnetic transi-

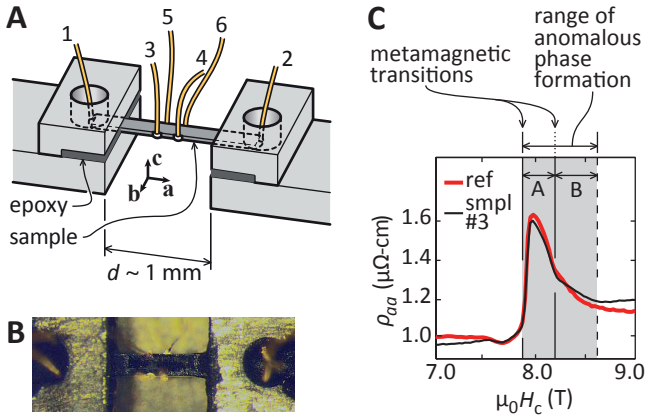

Figure 2: **Sample setup for strain tuning. A and B** Schematic illustration and photograph of a mounted sample. Strain is applied by minutely varying the gap width d. **C.** ρ_{aa} against H_c, where $\mathbf{H} = (0, 0, H_c)$, of a zero-strain reference sample, and sample #3 mounted in the strain apparatus and tuned to near-zero strain. $T \approx 300$ mK. The ranges of the A and B phases are indicated.

tion fields of $Sr_3Ru_2O_7$, [34, 35] while uniaxial pressure along the c axis reduces the transition fields and eventually induces ferromagnetism. [36] In-plane uniaxial pressure experiments have not been reported, however a theoretical study found that nematic transitions may show first-order Griffiths wings in the presence of applied anisotropy. [37]

We apply in-plane uniaxial pressure using a piezoelectric-based apparatus that can both compress and tension test samples. [38] To our knowledge, this capability is unique. The sample is prepared as a bar and secured across a gap of width ∼1 mm. The piezoelectric stacks strain the sample by minutely varying the width of this gap. A photograph and schematic of a mounted sample are shown in Fig. 2. Because the center of the sample is free, the transverse strains are set by the Poisson's ratios of $Sr_3Ru_2O_7$. Compression along $\hat{\mathbf{a}}$, for example, induces expansion along $\hat{\mathbf{b}}$, so the applied strain induces strong orthorhombic distortion.

High strain homogeneity is important to keep the transitions reasonably narrow as strain is applied. Therefore, samples are prepared with high length-to-width and length-to-thickness aspect ratios, to reduce bending and end effects. Also, within the mounts the bonding to the sample is (approximately) symmetric between the upper and lower surfaces: asymmetry in the mounts causes the sample to bend as strain is applied, imposing a strain gradient across the sample thickness. [38]

The neutron scattering peaks suggest, as noted, ⟨100⟩ principle axes for any C_2-symmetric order parameter components. Vector field transport data also suggest ⟨100⟩ principle axes: an in-plane field component along (100) induces strong resistive anisotropy between the (100) and (010) directions, whereas a (110) field induces very little (110)/(1$\bar{1}$0) anisotropy. [39] Therefore, in the strain measurements the samples are cut, and the pressure applied, along a ⟨100⟩ axis. (That is, an Ru-O-Ru bond direction.) Three samples were strained. They were cut from the same crystal, because our aim was more to test reproducibility in mounting conditions than crystal-to-crystal variation, and the parent crystal has previously been thoroughly characterized with transport, magnetization, and de Haas-van Alphen experiments. [40] Six electrical contacts were made to each, as illustrated in Fig. 2A. Longitudinal resistivity ρ_{aa} was measured by running a current through contacts 1 and 2 and measuring

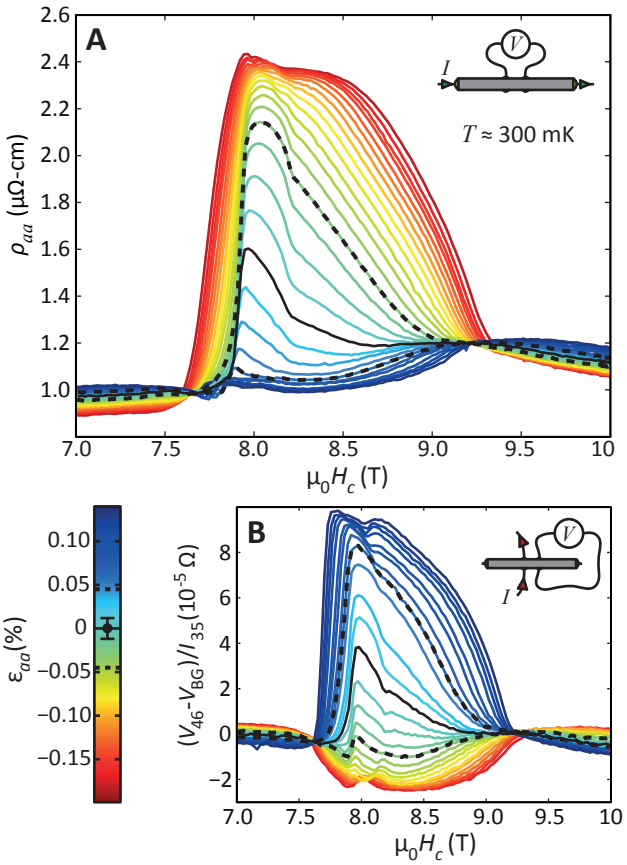

Figure 3: **Strain tuning results.** **A** Longitudinal resistivity ρ_{aa} against c-axis field for sample #3, at a series of applied sample strains. $\mathbf{H} = (0, 0, H_c)$, $T \approx 300$ mK. The measurement configuration is shown at top right. **B** Transverse response for the same sample. V_{46} is the voltage between contacts 4 and 6, V_{BG} the background, determined by fits to V_{46} outside the region of phase formation, and I_{35} is the current between contacts 3 and 5. Contact numbering is shown in Fig. 2A.

the voltage between contacts 5 and 6, or 3 and 4; the zero-field residual resistivity of the samples was ≈0.5 $\mu\Omega$-cm. A qualitative measure of the transverse resistivity, ρ_{bb}, could be obtained by passing current through contacts 3 and 5 and measuring voltage between contacts 4 and 6. It is only qualitative because: (i) The current flow is not homogeneous, so the measured voltage has some dependence on ρ_{aa}; and (ii) The transverse signal appeared on top of a field-dependent but strain-independent background, that prevented accurate calculations to extract ρ_{bb}. (This background was later found to originate in mechanical vibration of the transverse leads.)

Fig. 2C shows ρ_{aa} against field for a zero-strain reference sample, cut from the same original crystal as the strained samples and mounted on flexible wires to avoid thermal stresses. We compare with this reference to determine when the strained samples are at zero strain, to within an estimated error of ±0.01% strain. [41] Phase formation occurs between 7.9 and ≈8.6 T. The lower boundary coincides with the first metamagnetic transition. There is a clear resistive anomaly associated with the second metamagnetic transition at ≈8.1 T. The second transition separates regions of the phase denoted A and B; the existence of the B region was suggested by transport [42] and thermal expansion [31] measurements, and subsequently confirmed by the neutron study. [29]

ρ_{aa} of strained sample #3 at a series of applied strains and $T \approx 300$ mK is shown in Fig. 3A. [43] Because domain formation and metastability are possible with spontaneous symmetry breaking, the strain was incremented at 7 T, outside the field range for phase formation, and not varied while within the phase. ρ_{aa} increases strongly when the sample is compressed. Also, the range of fields over which ρ_{aa} is enhanced expands: under 0.2% compression phase formation, as identified by enhanced ρ_{aa}, extends from 7.7 to 9.3 T. In the two-component scenario, the effect of compression along $\hat{\mathbf{a}}$ is to increase $|\Delta_a|^2$, and expand the range over which $|\Delta_a|^2 > 0$. Tension on the other hand rapidly reduces the resistive response of the phase, and by 0.05% tension it is completely eliminated. The metamagnetic transition fields, as identified by their associated resistive anomalies, do not move dramatically. It will be useful in the future to probe the strain dependence of the metamagnetic transitions with magnetic measurements; if the resistive anomalies do indeed track the metamagnetic transitions, then clearly it is the B portion of the phase that expands dramatically under compression.

The transverse response (after subtraction of the background) is shown in panel B. It increases strongly when the sample is tensioned. This indicates strongly increased ρ_{bb}: although the transverse response is affected by ρ_{aa}, under strong tension ρ_{aa} is suppressed to a nearly constant base value. Compression along $\hat{\mathbf{a}}$ increases ρ_{aa}, and tension along $\hat{\mathbf{a}}$ increases ρ_{bb}.

Fig. 4 shows contour plots of the longitudinal and transverse responses. (In addition, contour plots for sample #2 are shown in Supplemental Material.) They approximately mirror each other, and for each there is a well-defined region of strongly enhanced response. [44] In the two-component scenario, these regions are where, respectively, $|\Delta_a|^2$ and $|\Delta_b|^2$ are nonzero. Their approximate boundaries are shown in panel C; there is a range of overlap, with maximum width $\approx$0.08%. That is, the data suggest that in the ground state there is a well-defined, noninfinitesimal region where $|\Delta_a|^2$ and $|\Delta_b|^2$ are simultaneously nonzero.

We conclude our presentation of strain-tuning data by showing, in Fig. 5A, the effect of strain over a wider field range. At fields outside the phase formation region, the response to strain is nearly linear over the applied strain range. Plotted in the figure is the normalized linear coefficient of the elastoresistance, $(1/R)dR/d\varepsilon$, taken at strain $\varepsilon = 0$. [45] It includes a geometric contribution, due to the forced change in sample dimensions. For isotropic materials with Poisson's ratio ν this geometric contribution is $1 + 2\nu$, typically $\lesssim 2$, and for ordinary metals it is typically the dominant contribution. [46] In narrow band metals the change in hopping can substantially enhance the elastoresistance, as can electronic correlations. [20] $Sr_3Ru_2O_7$ is known to be both narrow-band and strongly correlated, consistent with the observation of $(1/R)dR/d\varepsilon \sim 20$ far from the phase. This is much smaller than the elastoresistance within the phase, but still large. Also notable in the data are crossing points, at 7.6 and 9.2 T, where the elastoresistance is zero. The data in Fig. 5B shows that at these points ρ_{aa} is almost perfectly strain-independent for $|\varepsilon|$ up to $\sim$0.1%. It will be interesting, in future, to examine thermodynamic properties in the vicinity of these crossing points.

Results: vector field

Another way to lift C_4 symmetry is with a vector magnetic field, $\mathbf{H} = (H_a, H_b, H_c)$. Recently-published vector field results showed that the high susceptibility to in-plane fields of the A phase is shared by the B phase, and also persists to temperatures well above that

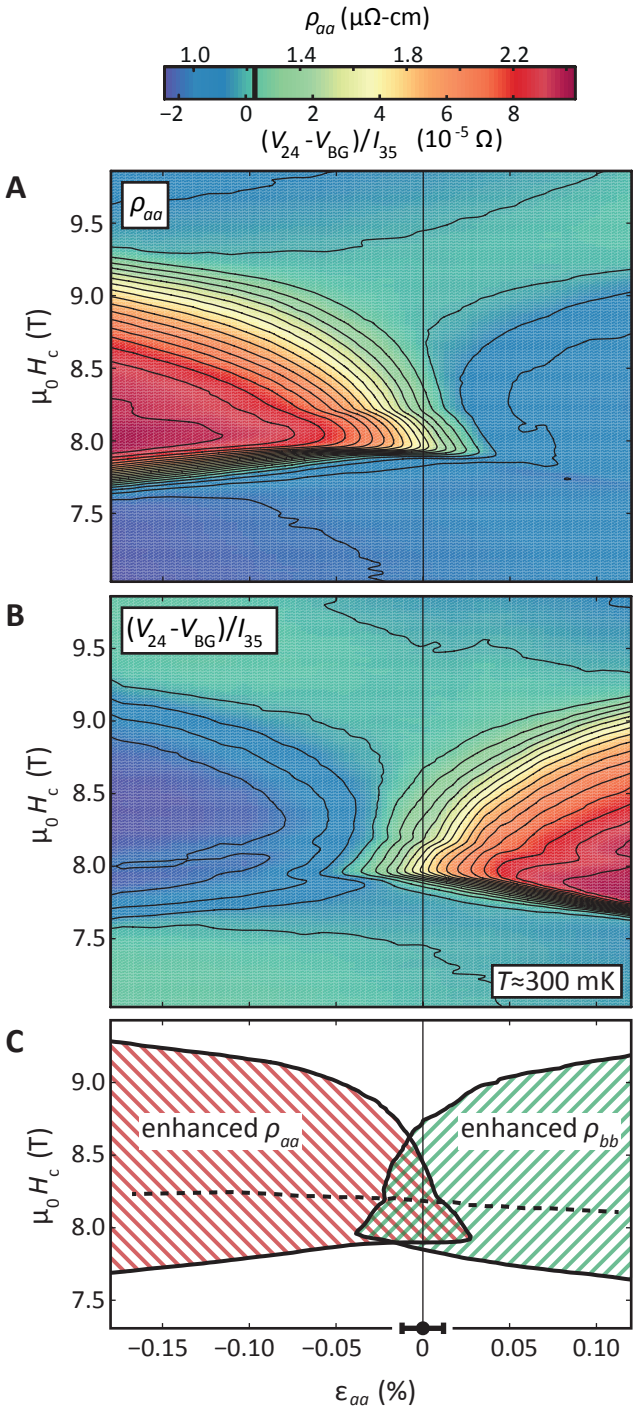

Figure 4: **Strain tuning contour plots.** **A** and **B**: Contour plots of the longitudinal and transverse response, respectively, of sample #3 as a function of c-axis magnetic field and sample strain. $\mathbf{H} = (0, 0, H_c)$, $T \approx 300$ mK. **C** Outlines of the regions of enhanced ρ_{aa} and ρ_{bb}. These outlines are taken, for convenience, as the contour level indicated by the heavy black line in the scale bar. The error bar on the x axis indicates the error in our determination of zero strain; by symmetry, if $\mathbf{H}$ is perfectly aligned with $\hat{\mathbf{c}}$ the borders of the enhanced-ρ_{aa} and enhanced-ρ_{bb} regions should cross at zero strain. The dashed line indicates the second metamagnetic transition, determined from its associated resistive anomaly.

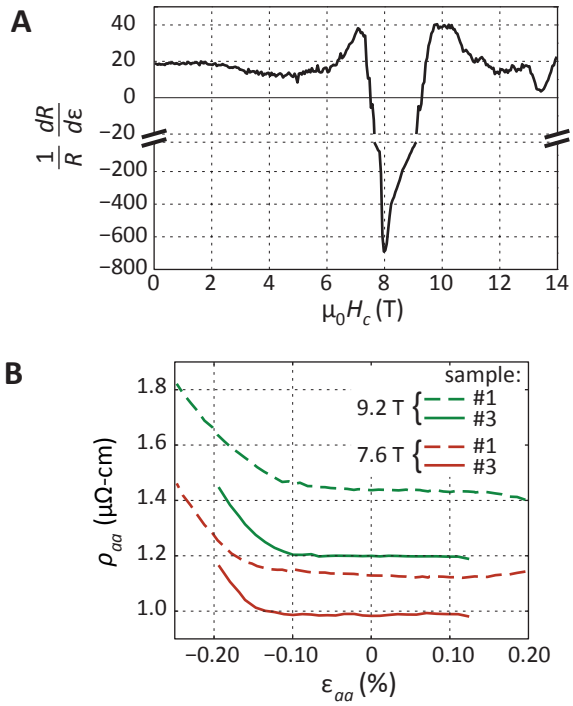

Figure 5: **Elastoresistance.** **A** Elastoresistance $(1/R)dR/d\varepsilon$ against magnetic field for sample #1. $\mathbf{H} = (0, 0, H_c)$, $T \approx 300$ mK. **B** ρ_{aa} against strain at 7.6 and 9.2 T. At these fields, ρ_{aa} is nearly independent of strain over a wide range of strain.

for phase formation. [42]

The vector magnet used in this study can apply H_c up to 8.5 T, simultaneously with $\sqrt{H_a^2 + H_b^2}$ up to 0.9 T. Therefore the field angle can be swept across a range $\approx \arctan(0.9/8.5) - \arctan(-0.9/8.5) = 12°$. Samples were mounted on a mechanical rotator to allow the sample c axis to be shifted relative to this accessible range.

A major phenomenological difference between vector field and strain is that, at lowest order, the coupling to $|\Delta_a|^2$ and $|\Delta_b|^2$ will be linear in strain but quadratic in in-plane field, because the response should be symmetric with respect to the sign of $H_{a,b}$. In a Ginzburg-Landau free energy functional of a two-component order parameter, the lowest-order coupling terms to in-plane field are $r_1(|\Delta_a|^2 H_a^2 + |\Delta_b|^2 H_b^2) + r_2(|\Delta_a|^2 H_b^2 + |\Delta_b|^2 H_a^2)$, where r_1 and r_2 are coupling constants.

The sample configuration for this measurement is illustrated in Fig. 6. As in Ref. [47], the sample is cut into an octagon, to provide shape symmetry between the a and b axes, and also between $\langle 100 \rangle$ and $\langle 110 \rangle$ directions. It is mounted on flexible wires to avoid strain effects. ρ_{aa} can be measured, approximately, by applying current through contacts 1 and 5 and measuring the voltage between contacts 2 and 4, or 8 and 6. Rotating the contacts by 90° yields, approximately, ρ_{bb}. The measures are approximate because the current flow is not completely homogeneous, leading to some cross-talk between ρ_{aa} and ρ_{bb}. However the shape symmetry makes it unambiguous whether a prominent feature is due primarily to a change in ρ_{aa} or ρ_{bb}. Three samples were measured in the vector magnet: two octagons, and also a high-aspect-ratio sample optimized for sensitivity to ρ_{aa}. Although the data presented is from the octagons, our conclusions are supported by all three samples independently.

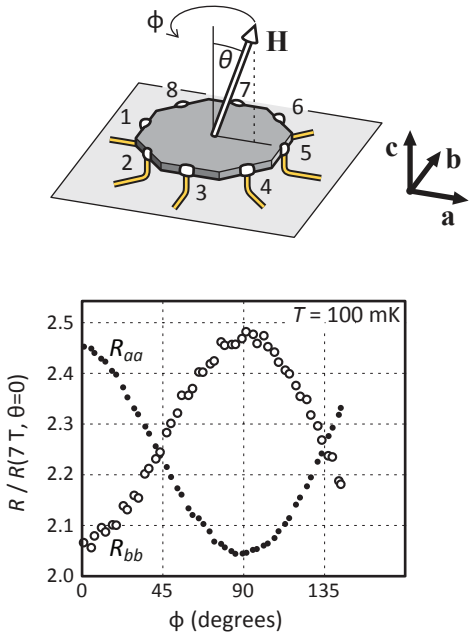

Figure 6: **Vector field sample configuration, and resistance against ϕ.** Top: sample and electrical contact configuration for the octagonal samples. Bottom: R_{aa} and R_{bb} against ϕ, with θ fixed at 6° and $|\mathbf{H}|$ fixed at 7.83 T. $R_{aa} = (V_2 - V_4)/I_{15}$, and $R_{bb} = (V_4 - V_6)/I_{37}$.

We start with the data presented in Fig. 6. $R_{aa} = (V_2 - V_4)/I_{15}$ and $R_{bb} = (V_4 - V_6)/I_{37}$ were measured while rotating $\mathbf{H}$ about $\hat{\mathbf{c}}$ at a fixed polar angle $\theta = 6°$. Both quantities vary approximately as $\cos(2\phi)$. Field rotation studies on the high-aspect-ratio sample, for θ between 1° and 10.5°, also showed a smooth dependence of ρ_{aa} on ϕ, and $\propto\cos(2\phi)$ at small θ.

This smooth dependence of R_{aa} and R_{bb} on ϕ does not match expectations for spontaneous symmetry breaking. With spontaneous C_2 symmetry, sharp steps are expected when the orientation of the order flips. (The pinning of field-induced anisotropy to $\langle 100\rangle$ directions means that any spontaneously C_2-symmetric order is expected to be Ising-type, *i.e.* not continuously rotatable.) If the order is broken up into domains then the reorientation of individual domains may yield a series of sharp jumps, known in ferromagnets as Barkhausen jumps. Similarly, flipping domains may be the origin of anomalous noise observed in $YBa_2Cu_3O_{7-\delta}$. [48, 49] However Barkhausen-like jumps are not evident in the data on $Sr_3Ru_2O_7$, and the magnitude of the noise within the phase was the same as outside.

A $\cos(2\phi)$ dependence follows immediately from a two-component order with $|\Delta_a| = |\Delta_b|$ at $H_{a,b} = 0$, and quadratic dependence on $H_{a,b}$: if the resistivity ρ_{aa} is linear in $|\Delta_a|^2$ over the measured range of $H_{a,b}$ then ρ_{aa} will be linear in $r_1 H_a^2 + r_2 H_b^2 = (r_1 \sin^2(\phi) + r_2 \cos^2(\phi))|\mathbf{H}|^2 \cos^2(\theta)$, which is linear in $\cos(2\phi)$.

Therefore the $\cos(2\phi)$ form of R_{aa} and R_{bb} argues in favor of C_4 symmetry at $H_{a,b} = 0$. However, it is possible that Barkhausen jumps are not evident only because the domains of a C_2 order are small, so for more complete evidence on the symmetry of the order parameter we map R_{aa} and R_{bb} against H_a and H_c (keeping $H_b = 0$). R_{aa} was measured while sweeping $|\mathbf{H}|$ through the phase at fixed θ, then R_{bb} in a second $|\mathbf{H}|$ sweep at the same θ, and then

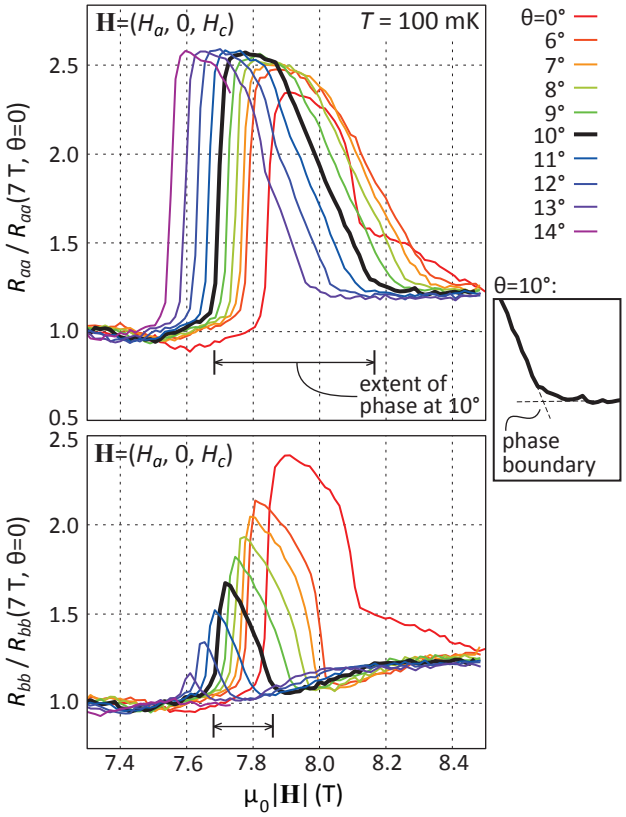

Figure 7: **Resistance against θ and $|\mathbf{H}|$.** R_{aa} and R_{bb} against $|\mathbf{H}|$ at various field angles $\theta = \tan^{-1}(H_a/H_c)$. $T = 100$ mK. The phase boundaries at $\theta = 10°$ are highlighted as an example.

θ was incremented. θ was not changed while within the ordered phase, to avoid inducing possible metastable domain configurations.

Results of measurements at nine nonzero values of θ are shown in Fig. 7. The vector field and strain measurements are complementary: although strain perturbs the phase much more strongly than in-plane field, the transitions remain sharper in the vector field data. This can be seen in Fig. 7, where the transitions in the vector field data can be readily identified by the changes in slope of R against $|\mathbf{H}|$. Contour plots of R_{aa} and R_{bb} are shown in Fig. 8A, with the transitions indicated by black points, [50] and Fig. 8B shows a vector field phase diagram. As in the strain phase diagram, there are distinct and well-defined regions over which ρ_{aa} and ρ_{bb} are enhanced. In the two-component scenario, these are regions, respectively, of nonzero $|\Delta_a|^2$ and $|\Delta_b|^2$. There is a region of overlap where $|\Delta_a|^2$ and $|\Delta_b|^2$ appear to be simultaneously nonzero.

The vector magnet is also an ideal tool to search for the hysteresis expected if there is spontaneous symmetry breaking, because it does not heat the sample. Results of one test, in which R_{bb} was measured while increasing then decreasing H_a, are shown in Fig. 9. H_c was simultaneously controlled to stay within the coexistence region, up to $\mu_0 H_a \approx 1.5$ T. It is well-established in the data above that H_a favors Δ_a, so if Δ_a and Δ_b do not co-exist microscopically, and the phase is exited and re-entered at strong H_a, Δ_b domains are not expected to re-form. However the data show no resolvable hysteresis: on ramping H_a back downward, enhanced ρ_{bb} is re-established at exactly the same field (within resolution) where it was suppressed on the upward ramp. This test was performed at 50 mK, a factor of twenty

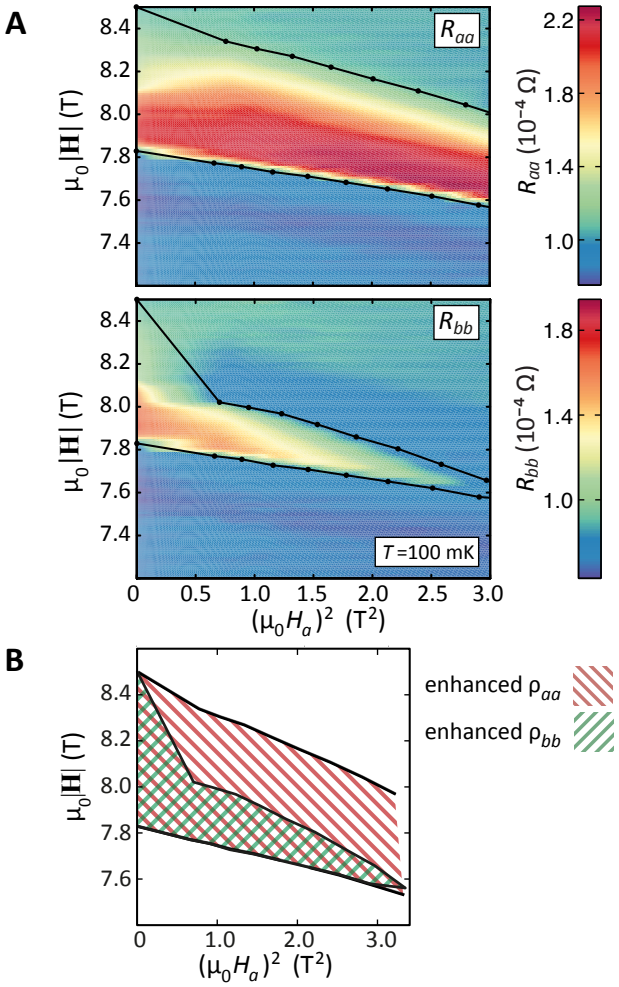

Figure 8: **Vector field results: contour plots.** **A** R_{aa} and R_{bb} against $|\mathbf{H}|$ and H_a^2, with $\mathbf{H} = (H_a, 0, H_c)$, at $T = 100$ mK. The black points indicate phase boundaries. **B** Outlines of the regions of enhanced ρ_{aa} and ρ_{bb}.

lower than the transition temperature into the phase.

Another test for hysteresis consisted of in-plane field rotations, as illustrated in Fig. 6, with clockwise and counter-clockwise rotation. The rotations were performed at values of θ between 6° and 14°, and spanned $\phi = 45°$, where, for spontaneous C_2 symmetry, the applied field should start to flip domains between (100) and (010) orientations. Again, no definite hysteresis was observed.

Discussion

Both the strain and vector field phase diagrams show well-defined, noninfinitesimal regions of overlap, within which both ρ_{aa} and ρ_{bb} are enhanced. The overlap regions were repeatedly exited and re-entered in the presence of applied C_2 fields. Therefore, they appear to be an intrinsic, ground-state property.

This result, previous vector field data, and the neutron scattering data are all consistent with a two-component model, within which the enhancements in ρ_{aa} and ρ_{bb} are monotonic functions of order parameter magnitudes $|\Delta_a|^2$ and $|\Delta_b|^2$, respectively, and Δ_a and Δ_b can

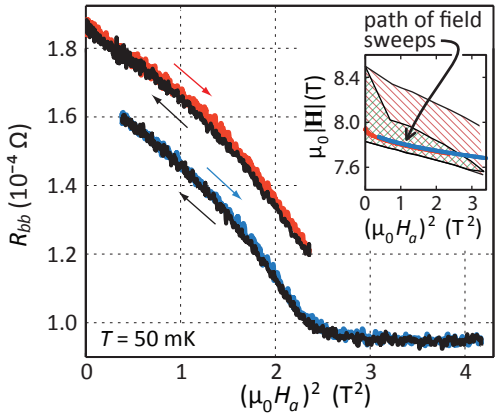

Figure 9: **Looking for hysteresis.** Two demonstrations of the absence of hysteresis. The upper curves are offset by $2 \cdot 10^{-5}$ Ω for clarity. $I = 100$ μA, $\mathbf{H} = (H_a, 0, H_c)$, $T = 50$ mK. As shown in the inset, H_c was varied while H_a was ramped to keep the sample within the enhanced-ρ_{bb} phase up to $(\mu_0 H_a)^2 \approx 2.3$ T^2.

coexist microscopically in the ground state. With microscopic coexistence, it is very likely that $|\Delta_a| = |\Delta_b|$ in the absence of a C_4-symmetry-breaking field, yielding a C_4-symmetric state. (D_{2d} symmetry is also possible; this is discussed later.) In terms of the density wave order, this means microscopically coexisting perpendicular density waves, similar to the perpendicular charge density waves observed in some rare-earth tri-telluride compounds, [51, 52] and the tetragonal spin density wave state recently discovered in iron pnictide superconductors. [53] This is all similar to $p_x \pm ip_y$ in Sr2RuO4. [54, 55]

It is evident from Fig. 4, and the fact that the order condenses only at low temperatures and only over a narrow field range, that the order is only weakly stabilized in the unstrained lattice. It is therefore reasonable that its two components respond strongly to perturbation, yielding a high susceptibility to C_2-symmetric fields.

This proposal of microscopic coexistence is in contrast to the currently prevailing hypothesis for $Sr_3Ru_2O_7$, which is domains of locally C_2-symmetric order. We now argue that domain formation cannot straightforwardly account for our observations. As noted in the Introduction, ground-state domains might be favored due to random-field disorder and/or long-range interactions; we consider these possibilities in turn.

Random-field disorder should in general yield ground-state domain formation over a range of applied C_2 field approximately matching the range of the inhomogeneity, and should broaden the bulk transitions on a similar scale. However what is seen in the vector field data, most clearly in Fig. 9, is sharp transitions into a broad coexistence region. This is a natural result of microscopic coexistence, but not of inhomogeneity-induced broadening. In the strain data, although the transitions are not as sharp as in the vector field data, at a maximum width of ≈0.08% strain the coexistence region is broad on the scale of the rounding on the transitions. Furthermore, as seen in Fig. 4C the width of the coexistence region varies with H_c, which is not expected if it were set by a field-independent strain distribution.

Long-range elastic interactions could stabilize domains because the strain applied by the apparatus is an *average* strain across the length of the sample. If a C_2-symmetric electronic order induces C_2 lattice deformation exceeding the applied average strain, elastic interac-

tions favor domain formation. However this mechanism is not quantitatively consistent with observations. The C_2 lattice distortion induced by tilting the applied field to $\theta = 15°$ (more than enough to exit the coexistence region and fully orient the order, if there are domains) is $|a-b|/(a+b) \sim 4 \cdot 10^{-6}$. [32] That is, if there is spontaneous C_2 symmetry, elastic interactions might favour domain formation up to an applied average strain of $\sim 4 \cdot 10^{-6}$. However the observed coexistence region extends to strains of $\sim 4 \cdot 10^{-4}$.

Similarly, although magnetic dipole interactions could favor domain formation if the domains have differing magnetizations, [56] the coexistence region extends up to a rather strong in-plane field of $\mu_0 H_a = 1.7$ T. The order would need to include in-plane ferromagnetism on this scale to stabilize ground-state domains against the applied in-plane field. There is no expectation of that; for comparison, the larger metamagnetic jump, at 7.9 T, has a magnitude of $\mu_0 \Delta M = 0.008$ T. [30]

In summary, unless another mechanism to induce domains is identified, the coexistence appears to be microscopic, and therefore the order is likely to be C_4 symmetric in the absence of C_4-symmetry-breaking fields. It should however be noted that spontaneous C_2 symmetry is not strictly ruled out: although a lowest-order free energy analysis yields the zero-C_2-field possibilities that either $|\Delta_a| = |\Delta_b|$, or one of Δ_a and Δ_b is zero, it is also a logical possibility that there is spontaneous inequality between $|\Delta_a|$ and $|\Delta_b|$ where both remain nonzero. A sufficiently small spontaneous inequality would not be discernable in the data. Spontaneous inequality could emerge, *e.g.*, from coupling between the density wave order and an underlying nematic order.

Another point to note is that direct identification of resistivity enhancement with the amplitude of an order parameter is at odds with much previous discussion on $Sr_3Ru_2O_7$. When the order parameter was generally though to be nematic order alone, domain wall scattering was thought necessary to explain the magnitude of the resistivity enhancement, because plausible nematic Fermi surface distortions are not expected to yield large changes in resistivity. [57] The near temperature independence of the resistivity within the phase, [15] indicating a constant mean free path, also suggests domain walls, as does the anomalous suppression of longer orbits seen in quantum oscillation data within the phase. [58] Density wave order, by gapping sections of Fermi surface, should generally yield larger intrinsic resistivity changes than C_2 Fermi surface distortions. Even so, the magnitude of the enhancement remains surprising: at large strains, the ratio of resistivities parallel and perpendicular to the density wave $\rho_\parallel/\rho_\perp$ saturates at $\sim$2.5. For comparison, in elemental chromium, a three-dimensional metallic spin density wave system with $T_N = 312$ K, $\rho_\parallel/\rho_\perp$ saturates at only 1.08. [59] $Sr_3Ru_2O_7$ has at least seven Fermi surface sheets, and it does not appear possible that nesting across a single wave vector could gap away enough carriers to explain such strong anisotropy. Widespread gapping also appears inconsistent with observed thermodynamic properties: the entropy as $T \to 0$ is highest in the region of phase formation, indicating a large number of ungapped carriers. [60, 30, 61]

Therefore, there is still a reason to suspect domain wall scattering is important, although it is now very unclear what the origin of domain walls might be. A model where ρ_{aa} and ρ_{bb} are direct functions of order parameter magnitudes $|\Delta_a|^2$ and $|\Delta_b|^2$ is qualitatively simple and consistent with the data. Models producing strong resistivity enhancement through domain wall scattering, but no resolvable hysteresis, seem likely to require considerable complexity and fine-tuning.

We conclude by noting that although the discussion in this paper has been about C_4 versus spontaneous C_2 symmetry, D_{2d} point-group symmetry has also been proposed for $Sr_3Ru_2O_7$, [62, 63, 64] and may be consistent with our data. It is also proposed for cuprate superconductors. [65] This is an inversion-symmetry-breaking point group, with (100)-oriented order in one layer of each bilayer, and (010)-oriented order in the other; the coexistence is microscopic but spatially separated. D_{2d} order also permits domain walls, across which the (100) and (010) layers are switched, although as with C_2 domains the absence of hysteresis seems inconsistent with domain walls being the main source of bulk resistivity.

In summary, we have presented the results of an extensive experimental study of the resistive response of the low-temperature phase of $Sr_3Ru_2O_7$ to C_4-symmetry-breaking in-plane strain and magnetic fields. Although spontaneous C_2 symmetry is not strictly ruled out, the results are all qualitatively explainable with a two-component order parameter, where the components coexist microscopically over a noninfinitesimal range of applied C_2-symmetric fields. The data are not consistent with straightforward models for domains of (100) and (010) order. The microscopic coexistence suggests C_4 symmetry in the absence of any C_4-symmetry-breaking fields, although D_{2d} symmetry is also a possibility.

Materials and Methods

Samples were grown by a floating zone method. [66] Samples were cut to the desired shape with a wire saw. The strained samples were 40–45 μm thick and between 170 and 280 μm wide. Electrical contacts were made with DuPont 6838 silver paste, cured at 450° C for ≈ 5 minutes. The strained samples were secured in the strain apparatus with Stycast 2850, cured at a temperature of $\sim 65°$ for several hours to obtain a harder cure than at room temperature. For samples 1, 2, and 3, the epoxy thickness on either wide of the sample was $\sim$80, 40, and 20 μm, respectively. For low-noise measurements of resistivity, on strained sample #1 and for the vector field data we used low-temperature transformers to amplify the signal voltage. For samples #2 and #3, room-temperature transformers were used.

Strained sample #1 was mounted in the same strain apparatus reported in Refs. [38] and [54], which used a strain gauge for measurement of the displacement applied to the sample. Samples #2 and #3 were mounted in a newer apparatus with a capacitive displacement sensor. Through comparison of the elastoresistive response of $Sr_3Ru_2O_7$ outside the region of phase formation it was found that strains reported from the original apparatus needed to be multiplied by a factor of 1.6 to match those reported from the newer apparatus, suggesting that the strain gauge substantially impeded the motion of the original apparatus. This correction factor was also verified with measurements in Sr_2RuO_4, and is included in all strains reported for sample #1.

We performed finite element calculations to estimate that, for the three samples, 52%, 68%, and 78%, respectively, of the applied displacement was transmitted to exposed portion of the sample as sample strain. For these calculations, we took the Young's modulus of the epoxy to be 15 GPa, and for $Sr_3Ru_2O_7$ we took the elastic tensor of Sr_2RuO_4. [67]

References

[1] A. Tamai, M.P. Allan, J.F. Mercure, W. Meevasana, R. Dunkel, D.H. Lu, R.S. Perry, A.P. Mackenzie, D.J. Singh, Z.-X. Shen, and F. Baumberger. Fermi Surface and van Hove Singularities in the Itinerant Metamagnet $Sr_3Ru_2O_7$. *Phys. Rev. Lett.* **101** 026407 (2008).

[2] M.P. Allan, A. Tamai, E. Rozbicki, M.H. Fischer, J. Voss, P.D.C. King, W. Meevasana, S. Thirupathaiah, E. Rienks, J. Fink, D.A. Tennant, R.S. Perry, J.F. Mercure, M.A. Wang, Jinho Lee, C.J. Fennie, E.-A. Kim, M.J. Lawler, K.M. Shen, A.P. Mackenzie, Z.-X. Shen, and F. Baumberger. Formation of heavy d-electron quasiparticles in $Sr_3Ru_2O_7$. *New Journal of Physics* **15** 063029 (2013).

[3] S.-I. Ikeda, Y. Maeno, S. Nakatsuji, M. Kosaka, and Y. Uwatoko. Ground state in $Sr_3Ru_2O_7$: Fermi liquid close to a ferromagnetic instability. *Phys. Rev. B* **62** R6089 (2000).

[4] L. Capogna, E.M. Forgan, S.M. Hayden, A. Wildes, J.A. Duffy, A.P. Mackenzie, R.S. Perry, S. Ikeda, Y. Maeno, and S.P. Brown. Observation of two-dimensional spin fluctuations in the bilayer ruthenate $Sr_3Ru_2O_7$ by inelastic neutron scattering. *Phys. Rev. B* **67** 012504 (2003).

[5] R. Mathieu, A. Asamitsu, Y. Kaneko, J.P. He, X.Z. Yu, R. Kumai, Y. Onose, N. Takeshita, T. Arima, H. Takagi, and Y. Tokura. Impurity-induced transition to a Mott insulator in $Sr_3Ru_2O_7$. *Phys. Rev. B* **72** 092404 (2005).

[6] M.A. Hossain, B. Bohnenbuck, Y.D. Chuang, M.W. Haverkort, I.S. Elfimov, A. Tanaka, A.G. Cruz Gonzalez, Z. Hu, H.-J. Lin, C.T. Chen, R. Mathieu, Y. Tokura, Y. Yoshida, L.H. Tjeng, Z. Hussain, B. Keimer, G.A. Sawatzky, and A. Damascelli. Mott versus Slater-type metal-insulator transition in Mn-substituted $Sr_3Ru_2O_7$. *Phys. Rev. B* **86** 041102 (2012).

[7] A.P. Mackenzie, J.A.N. Bruin, R.A. Borzi, A.W. Rost, and S.A. Grigera. Quantum criticality and the formation of a putative electronic liquid crystal in $Sr_3Ru_2O_7$. *Physica C* **481** 207 (2012).

[8] S.A. Grigera, P. Gegenwart, R.A. Borzi, F. Weickert, A.J. Schofield, R.S. Perry, T. Tayama, T. Sakakibara, Y. Maeno, A.G. Green, A.P. Mackenzie. Disorder-Sensitive Phase Formation Linked to Metamagnetic Quantum Criticality. *Science* **306** 1154 (2004).

[9] S.A. Grigera, R.A. Borzi, A.P. Mackenzie, S.R. Julian, R.S. Perry, and Y. Maeno. Angular dependence of the magnetic susceptibility in the itinerant metamagnet $Sr_3Ru_2O_7$. *Phys. Rev. B* **67** 214427 (2003).

[10] A.G. Green, S.A. Grigera, R.A. Borzi, A.P. Mackenzie, R.S. Perry, and B.D. Simons. Phase Bifurcation and Quantum Fluctuations in $Sr_3Ru_2O_7$. *Phys. Rev. Lett.* **95** 086402 (2005).

[11] H.-Y. Kee and Y.B. Kim. Itinerant metamagnetism induced by electronic nematic order. *Phys. Rev. B* **71** 184402 (2005).

[12] H. Yamase. Mean-field theory on a coupled system of ferromagnetism and electronic nematic order. *Phys. Rev. B* **87** 195117 (2013).

[13] A.M. Berridge, A.G. Green, S.A. Grigera, and B.D. Simons. Inhomogeneous Magnetic Phases: A Fulde-Ferrell-Larkin-Ovchinnikov-Like Phase in $Sr_3Ru_2O_7$. *Phys. Rev. Lett.* **102** 136404 (2009).

[14] A.M. Berridge, S.A. Grigera, B.D. Simons, and A.G. Green. Magnetic analog of the Fulde-Ferrell-Larkin-Ovchinnikov phase in $Sr_3Ru_2O_7$. *Phys. Rev. B* **81** 054429 (2010).

[15] R.A. Borzi, S.A. Grigera, J. Farrell, R.S. Perry, S.J.S. Lister, S.L. Lee, D.A. Tennant, Y. Maeno, and A.P. Mackenzie. Formation of a Nematic Fluid at High Fields in $Sr_3Ru_2O_7$. *Science* **315** 214 (2007).

[16] The space group of $Sr_3Ru_2O_7$ is Bbcb: cooperative rotations of the RuO_6 octahedra formally reduce the lattice symmetry from tetragonal to orthorhombic, [68] with the principle axes oriented at 45° relative to the Ru-O-Ru bond directions. A convergent electron beam diffraction measurement found orthorhombic domains, [69] while later neutron diffraction results were best modelled with the tetragonal cell. [70] No effect of the orthorhombicity on electronic structure has been found, and in principle the orthorhombicity should not induce anisotropy between the Ru-O-Ru bond directions. Therefore, for convenience, in this article we refer to $Sr_3Ru_2O_7$ as tetragonal.

[17] Y. Ando, K. Segawa, S. Komiya, and A.N. Lavrov. Electrical Resistivity Anisotropy from Self-Organized One Dimensionality in High-Temperature Superconductors. *Phys. Rev. Lett.* **88** 137005 (2002).

[18] V. Hinkov, D. Haug, B. Fauqué, P. Bourges, Y. Sidis, A. Ivanov, C. Bernhard, C.T. Lin, B. Keimer. Electronic Liquid Crystal State in the High-Temperature Superconductor $YBa_2Cu_3O_{6.45}$. *Science* **319** 597 (2008).

[19] J.-H. Chu, J.G. Analytis, K. De Greeve, P.L. McMahon, Z. Islam, Y. Yamamoto, and I.R. Fisher. In-Plane Resistivity Anisotropy in an Underdoped Iron Arsenide Superconductor. *Science* **329** 824 (2010).

[20] J.-H. Chu, H.-H. Kuo, J.G. Analytis, and I.R. Fisher. Divergent Nematic Susceptibility in an Iron Arsenide Superconductor. *Science* **337** 710 (2012).

[21] J. Pollanen, K.B. Cooper, S. Brandsen, J.P. Eisenstein, L.N. Pfeiffer, and K.W. West. Heterostructure symmetry and the orientation of the quantum Hall nematic phases. *Phys. Rev. B* **92** 115410 (2015).

[22] M.P. Lilly, K.B. Cooper, J.P. Eisenstein, L.N. Pfeiffer, and K.W. West. Evidence for an Anisotropic State of Two-Dimensional Electrons in High Landau Levels. *Phys. Rev. Lett.* **82** 394 (1999).

[23] R. Okazaki, T. Shibauchi, H.J. Shi, Y. Haga, T.D. Matsuda, E. Yamamoto, Y. Onuki, H. Ikeda, and Y. Matsuda. Rotational Symmetry Breaking in the Hidden-Order Phase of URu_2Si_2. *Science* **331** 439 (2011).

[24] H. Yamase and A.A. Katanin. Van Hove Singularity and Spontaneous Fermi Surface Symmetry Breaking in $Sr_3Ru_2O_7$. *J. Phys. Soc. Japan* **76** 073706 (2007).

[25] W.-C. Lee and C.-J. Wu. Theory of unconventional metamagnetic electron states in orbital band systems. *Phys. Rev. B* **80** 104438 (2009).

[26] S. Raghu, A. Paramekanti, E.A. Kim, R.A. Borzi, S.A. Grigera, A.P. Mackenzie, and S.A. Kivelson. Microscopic theory of the nematic phase in $Sr_3Ru_2O_7$. *Phys. Rev. B* **79** 214402 (2009).

[27] C.M. Puetter, J.G. Rau, and H.-Y. Kee. Microscopic route to nematicity in $Sr_3Ru_2O_7$. *Phys. Rev. B* **81** 081105(R) (2010).

[28] M. Tsuchiizu, Y. Ohno, S. Onari, and H. Kontani. Orbital Nematic Instability in the Two-Orbital Hubbard Model: Renormalization-Group + Constrained RPA Analysis. *Phys. Rev. Lett.* **111** 057003 (2013).

[29] C. Lester, S. Ramos, R.S. Perry, T.P. Croft, R.I. Bewley, T. Guidi, P. Manueal, D.D. Khalyavin, E.M. Forgan, and S.M. Hayden. Field-tunable spin-density-wave phases in $Sr_3Ru_2O_7$. *Nature Materials* **14** 373 (2015).

[30] A.W. Rost, R.S. Perry, J.F. Mercure, A.P. Mackenzie, and S.A. Grigera. Entropy Landscape of Phase Formation Associated with Quantum Criticality in $Sr_3Ru_2O_7$. *Science* **325** 1360 (2009).

[31] C. Stingl, R.S. Perry, Y. Maeno, and P. Gegenwart. Electronic nematicity and its relation to quantum criticality in $Sr_3Ru_2O_7$ studied by thermal expansion. *Physica Status Solidi B* **250** 450 (2013).

[32] C. Stingl, R.S. Perry, Y. Maeno, and P. Gegenwart. Symmetry-Breaking Lattice Distortion in $Sr_3Ru_2O_7$. *Phys. Rev. Lett.* **107** 026404 (2011).

[33] The lowest-order free energy functional of a two-component order parameter can be written $F = a(T - T_{c,0})(|\Delta_a|^2 + |\Delta_b|^2) + \beta_1(|\Delta_a|^4 + |\Delta_b|^4) + \beta_2|\Delta_a|^2|\Delta_b|^2 + ...$ If $\beta_2 > 2\beta_1$, Δ_a and Δ_b simultaneously nonzero is not a stable state, and at T_c either Δ_a or Δ_b condense. β_2 may be large if, *e.g.*, both components draw carriers from the same sections of Fermi surface.

[34] W. Wu, A. McCollam, S.A. Grigera, R.S. Perry, A.P. Mackenzie, and S.R. Julian. Quantum critical metamagnetism of $Sr_3Ru_2O_7$ under hydrostatic pressure. *Phys. Rev. B* **83** 045106 (2011).

[35] M. Chiao, C. Pfleiderer, S.R. Julian, G.G. Lonzarich, R.S. Perry, A.P. Mackenzie, Y. Maeno. Effect of pressure on metamagnetic $Sr_3Ru_2O_7$. *Physica B* **312-313** 698 (2002).

[36] S.-I. Ikeda, N. Shirakawa, T. Yanagisawa, Y. Yoshida, S. Koikegami, S. Koike, M. Kosaka, and Y. Uwatoko. Uniaxial-Pressure Induced Ferromagnetism of Enhanced Paramagnetic $Sr_3Ru_2O_7$. *J. Phys. Soc. Japan* **73** 1322 (2004).

[37] H. Yamase. Electronic nematic phase transition in the presence of anisotropy. *Phys. Rev. B* **91** 195121 (2015).

[38] C.W. Hicks, M.E. Barber, S.D. Edkins, D.O. Brodsky, and A.P. Mackenzie. Piezoelectric-based apparatus for strain-tuning. *Rev. Sci. Inst.* **85** 065003 (2014).

[39] J.A.N. Bruin, R. Borzi, S.A. Grigera, R.S. Perry, and A.P. Mackenzie. *in preparation.*

[40] J.-F. Mercure, A.W. Rost, E.C.T. OFarrell, S.K. Goh, R.S. Perry, M.L. Sutherland, S.A. Grigera, R.A. Borzi, P. Gegenwart, A.S. Gibbs, and A.P. Mackenzie. Quantum oscillations near the metamagnetic transition in $Sr_3Ru_2O_7$. *Phys. Rev. B* **81** 235103 (2010).

[41] In addition to the estimated $\pm 0.01\%$ error on the location of zero strain, we estimate a $\sim 20\%$ proportional error on strains quoted in this paper, due to uncertainty in how the epoxy securing the samples deforms as the strain is applied. However, no hysteresis against applied strain was observed, indicating that the sample and epoxy deformation was always elastic. Any overall scaling applied to the reported strains does not affect the conclusions of this paper.

[42] J.A.N. Bruin, R.A. Borzi, S.A. Grigera, A.W. Rost, R.S. Perry, and A.P. Mackenzie. Study of the electronic nematic phase of $Sr_3Ru_2O_7$ with precise control of the applied magnetic field vector. *Phys. Rev. B* **87** 161106(R) (2013).

[43] Due to field dependence of the temperature sensor, the temperature increases by ~ 20 mK between 7 and 10 T; this variation does not affect our conclusions.

[44] In the transverse response, there is also a broad shallow depression with compressive strains; this most likely is an artefact of sharply increased ρ_{aa} over this region. The important feature in the transverse response is the strong increase under tension, which can only be due to strongly enhanced ρ_{bb}.

[45] It would be useful to resolve the elastoresistance into the elastoresistive coefficients m_{11} and m_{12}, where $\Delta\rho_{aa} = m_{11}\varepsilon_{aa} + m_{12}\varepsilon_{bb}$. [46] $m_{12} \sim -m_{11}$, for example, would indicate strong nematic fluctuations. In the present experiment we cannot extract ρ_{bb} with sufficient precision, so this is future work.

[46] H.-H. Kuo, M.C. Shapiro, S.C. Riggs, and I.R. Fisher. Measurement of the elastoresistive coefficients of the underdoped iron arsenide $Ba(Fe_{0.975}Ca_{0.025})_2As_2$. *Phys. Rev. B* **88** 085113 (2013).

[47] R.A. Borzi, A. McCollam, J.A.N. Bruin, R.S. Perry, A.P. Mackenzie, and S.A. Grigera. Hall coefficient anomaly in the low-temperature high-field phase of $Sr_3Ru_2O_7$. *Phys. Rev. B* **84** 205112 (2011).

[48] D.S. Caplan, V. Orlyanchik, M.B. Weissman, D.J. Van Harlingen, E.H. Fradkin, M.J. Hinton, and T.R. Lemberger. Anomalous Noise in the Pseudogap Regime in $YBa_2Cu_3O_{7-\delta}$. *Phys. Rev. Lett.* **104** 177001 (2010).

[49] E.W. Carlson, K.A. Dahmen, E. Fradkin, and S.A. Kivelson. Hysteresis and Noise from Electronic Nematicity in High-Temperature Superconductors. *Phys. Rev. Lett.* **96** 097003 (2006).

[50] The prominent enhancements of R_{aa} and R_{bb} in Fig. 8A can be unambiguously assigned as changes in ρ_{aa} or ρ_{bb}. More subtle features are less clear. For example, in the lower panel R_{bb} is suppressed slightly when ρ_{aa} is strongly enhanced. This may be an artefact of the strong change in ρ_{aa}, not an effect in ρ_{bb}.

[51] N. Ru, C.L. Condron, G.Y. Margulis, K.Y. Shin, J. Laverock, S.B. Dugdale, M.F. Toney, and I.R. Fisher. Effect of chemical pressure on the charge density wave transition in rare-earth tritellurides RTe_3. *Phys. Rev. B* **77** 035114 (2008).

[52] R.G. Moore, V. Brouet, R. He, D.H. Lu, N. Ru, J.-H. Chu, I.R. Fisher, and Z.-X. Shen. Fermi surface evolution across multiple charge density wave transitions in $ErTe_3$. *Phys. Rev. B* **81** 073102 (2010).

[53] Xiaoyu Wang and R.M. Fernandes. Impact of local-moment fluctuations on the magnetic degeneracy of iron arsenide superconductors. *Phys. Rev. B* **89** 144502 (2014).

[54] C.W. Hicks, D.O. Brodsky, E.A. Yelland, A.S. Gibbs, J.A.N. Bruin, M.E. Barber, S.D. Edkins, K. Nishimura, S. Yonezawa, Y. Maeno, and A.P. Mackenzie. Strong Increase of T_c of Sr_2RuO_4 Under Both Compressive and Tensile Strain. *Science* **344** 283 (2014).

[55] M.B. Walker and P. Contreras. Theory of elastic properties of Sr_2RuO_4 at the superconducting transition temperature. *Phys. Rev. B* **66** 214508 (2002).

[56] B. Binz, H.B. Braun, T.M. Rice, M. Sigrist. Magnetic Domain Formation in Itinerant Metamagnets. *Phys. Rev. Lett.* **96** 196406 (2006).

[57] H.-J. Doh, Y.B. Kim, and K.H. Ahn. Nematic Domains and Resistivity in an Itinerant Metamagnet Coupled to a Lattice. *Phys. Rev. Lett.* **98** 126407 (2007).

[58] J.-F. Mercure, S. K. Goh, E.C.T. OFarrell, R.S. Perry, M.L. Sutherland, A.W. Rost, S.A. Grigera, R.A. Borzi, P. Gegenwart, and A.P. Mackenzie. Quantum Oscillations in the Anomalous Phase in $Sr_3Ru_2O_7$. *Phys. Rev. Lett.* **103** 176401 (2009).

[59] W.B. Muir and J.O. Ström-Olsen. Electrical Resistance if Single-Crystal Single-Domain Chromium from 77 to 325° K. *Phys. Rev. B* **4** 988 (1971).

[60] P. Gegenwart, F. Weickert, M. Garst, R.S. Perry, and Y. Maeno. Metamagnetic Quantum Criticality in $Sr_3Ru_2O_7$ Studied by Thermal Expansion. *Phys. Rev. Lett.* **96** 136402 (2006).

[61] A.W. Rost, S.A. Grigera, J.A.N. Bruin, R.S. Perry, D. Tian, S. Raghu, S.A. Kivelsone, and A.P. Mackenzie. Thermodynamics of phase formation in the quantum critical metal $Sr_3Ru_2O_7$. *Proc. Nat. Acad. Sciences* **108** 16549 (2011).

[62] C. Puetter, H. Doh, and H.-Y. Kee. Metanematic transitions in a bilayer system: Application to the bilayer ruthenate. *Phys. Rev. B* **76** 235112 (2007).

[63] H. Yamase. Spontaneous Fermi surface symmetry breaking in bilayer systems. *Phys. Rev. B* **80** 115102 (2009).

[64] T. Hitomi and Y. Yanase. Electric Octupole Order in Bilayer Ruthenate $Sr_3Ru_2O_7$. *J. Phys. Soc. Japan* **83** 114704 (2014).

[65] A.V. Maharaj, P. Hosur, and S. Raghu. Crisscrossed stripe order from interlayer tunneling in hole-doped cuprates. *Phys. Rev. B* **90** 125108 (2014).

[66] R. S. Perry and Y. Maeno. Systematic approach to the growth of high-quality single crystals of $Sr_3Ru_2O_7$. *J. Cryst. Growth*, **271** (2004).

[67] J.P. Paglione, C. Lupien, W.A. MacFarlane, J.M. Perz, L. Taillefer, Z.Q. Mao, and Y. Maeno. Elastic tensor of Sr_2RuO_4. *Phys. Rev. B* **65** 220506 (2002).

[68] H. Shaked, J.D. Jorgensen, O. Chmaissem, S. Ikeda, and Y. Maeno. Neutron Diffraction Study of the Structural Distortions in $Sr_3Ru_2O_7$. *J. Solid State Chemistry* **154** 361 (2000).

[69] R Kiyanagi, K Tsuda, N Aso, H Kimura, Y Noda, Y Yoshida, S Ikeda, and Y Uwatoko. Investigation of the Structure of Single Crystal $Sr_3Ru_2O_7$ by Neutron and Convergent Beam Electron Diffractions. *J. Phys. Soc. Japan* **73** 639 (2004).

[70] Biao Hu, G.T. McCandless, M. Menard, V.B. Nascimento, J.Y. Chen, E.W. Plummer, and R. Jin. Surface and bulk structural properties of single-crystalline $Sr_3Ru_2O_7$. *Phys. Rev. B* **81** 184104 (2010).

Acknowledgements

We acknowledge useful discussions with Joseph Betouras, Erez Berg, Rafael Fernandes, Andrew Green, Christopher Hooley, Steven Kivelson, and Walter Metzner. We thank the Max Planck Society and the EPSRC for financial support.

Author contributions: D.B. and M.B. carried out measurements on strain-tuning of $Sr_3Ru_2O_7$. J.B., R.B, and S.G. carried out the vector field measurements. R.P. grew the samples. A.M. and C.H. provided overall supervision. The manuscript was drafted by C.H., D.B., R.B., and J.B.

The data in this paper will be made available in Supplemental Material.

Supplemental Material

Fig. S1 shows the longitudinal and transverse responses for strained sample #2. The transverse response for this sample is simpler than with sample #3: we operated at a frequency where there was no substantial background to subtract off. However the transverse data are also noisier than for sample #3. These comments aside, as with sample #3 (Fig. 4), there is a small but definite region of overlap of enhanced ρ_{aa} and ρ_{bb}.

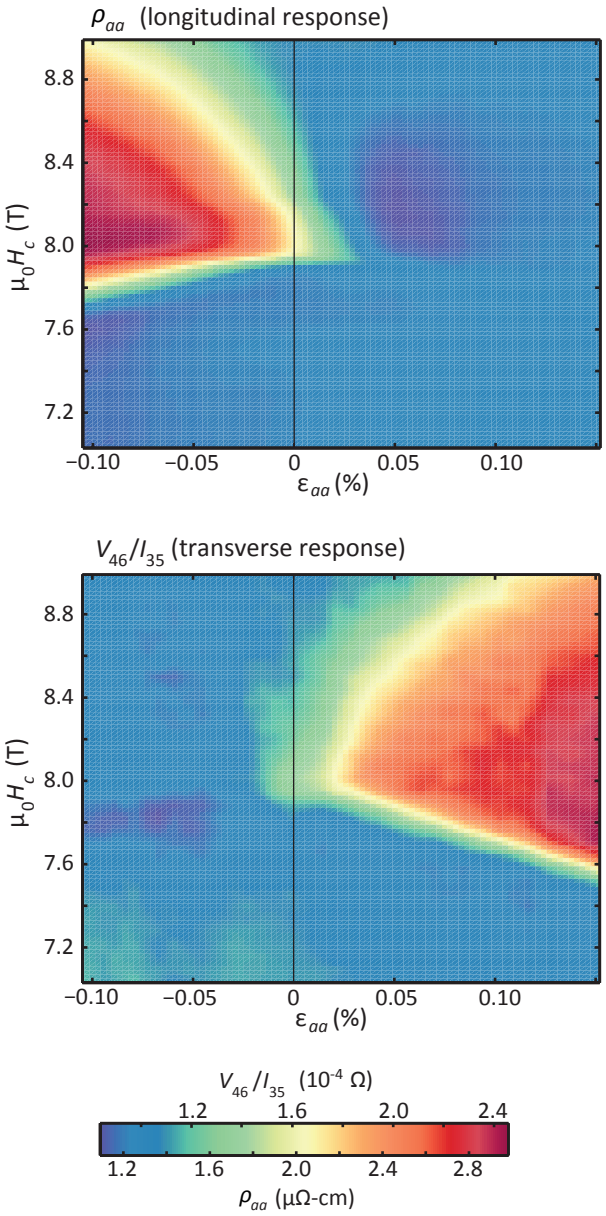

Figure S1: Longitudinal response and transverse response for strained sample #2.